The Eurasia Proceedings of Science, Technology, Engineering & Mathematics (EPSTEM)
ISSN: 2602-3199

The Eurasia Proceedings of Science, Technology, Engineering and Mathematics (EPSTEM), 2025

Volume 38, Pages 630-640

IConTES 2025: International Conference on Technology, Engineering and Science

Engineering Next Generation Hole Transport Layers for Lead Free Perovskite Solar Cells Exceeding 23% Power Conversion Efficiency

Souheyla Mamoun
University of Abou Bekr Belkaid

Abdelkrim Elhasnaine Merad
University of Abou Bekr Belkaid

Feryel Saidi
University of Abou Bekr Belkaid

Abstract: Lead-based halogenated perovskite solar cells have been mainly studied recently; however, these cells have two major drawbacks: lead toxicity and device instability, which limit their commercialization. In this paper, we investigate, theoretically, the effect of temperature on the PV performance of a lead-free perovskite solar cell (PSC) based on formamidinium tin iodide ($HC(NH_2)_2SnI_3$) in the configuration: FTO/WS_2/$HC(NH_2)_2SnI_3$/Cu_2O/Au. Three inorganic materials (CuSCN, MoO_3 and NiO) and three other organic materials (Spiro-OMeTAD, P3HT and D-PBTTT-14) were used as hole transport layers (HTL) and are also tested under temperature effect. Simulations showed that the introduction of CuSCN, Cu_2O, MoO_3 and NiO as (HTL) materials leads to a remarkable efficiency of 23.24% up to 389K which reflects the resistivity of these cells at such a high temperature. Substitution of the back contact layer metal by Pt, Ni and Pd metals can maintain this fixed efficiency, and among these alternatives Platinum may be the best candidate since it is both cheaper and non-toxic.

Keywords: Lead-free perovskite solar cell, SCAPS simulation, Inorganic and organic HTL, Working temperature effect, Back contact layer effect

Introduction

There are many space and terrestrial applications that can benefit from the development of photovoltaic devices that operate at high temperatures. As an example of terrestrial applications, we cite the hybrid photovoltaic-thermal solar collector. A space satellite close to the sun also requires robust solar cells that remain efficient at high temperatures. A satellite sent to Mercury would require photovoltaic (PV) cells operating at temperatures of about 450°C and light intensities ~10 times higher than in Earth orbit.

Therefore, developing PV cells for such applications introduces a number of challenges inherent to high-temperature operation. Increasing the temperature will increase the dark currents exponentially, leading to a significant reduction in the open-circuit voltage of the solar cell. High-temperature operation could also accelerate material degradation, reduce long-term reliability, and require the development of a stable metallization and cell encapsulation system. These challenges must, therefore, be carefully considered before any viable integration of PV cells into a system that requires high-temperature operation (Perl et al., 2016).

Photovoltaic technologies have attracted the attention of scientists because solar energy is considered clean and sustainable. In addition, the use of solar energy can help reduce environmental pollution due to fossil fuel consumption, as well as energy supply shortages. Therefore, perovskite solar cells (PSCs) based on

- Selection and peer-review under responsibility of the Organizing Committee of the Conference

organometallic halide have received global attention due to their outstanding properties such as very good absorption in a wide range of the light spectrum (Kwak et al., 2020), excellent charge carrier mobilities, low manufacturing cost [Li & Gao, 2020], and solution processing capability [Ashrafi et al., 2020; Zhang et al., 2020). Furthermore, since their first fabrication in 2009, the power conversion efficiency (PCE) of perovskite solar cells has increased considerably: it has gone from 3.4 to more than 27% (values obtained from the NREL chart as of October 31, 2025).

Lead halide perovskite solar cells have been widely used due to a number of attractive attributes: a tunable band gap (Filip et al., 2014; Sutton et al., 2016), a better light absorption coefficient, a high power PCE (Snaith et al., 2013), and long charge carrier diffusion lengths (Zhumekenov et al., 2016). However, despite these qualities and high PCEs of more than 20%, lead-based perovskite solar cells have two major drawbacks: device instability and lead toxicity (Kwak et al., 2020; Wang et al., 2017; Boopathi et al., 2017). To circumvent these drawbacks, various advances have been employed; for example, lead has been completely or partially replaced by other less toxic metals to form lead-free perovskites or metal-lead alloyed perovskites (Kamat et al., 2017).

Hu et al (Hu et al., 2020) designed a bismuth-based bulk heterojunction absorber material ($Cs_3Bi_2I_9$-$Ag_3Bi_2I_9$) to replace the lead halide absorber layer. The device achieved a PCE of 3.8% and exhibited improved thermal stability. Similarly, Kanoun et al (Kanoun et al., 2019) theoretically demonstrated the photovoltaic performance of a Germanium halide perovskite. The device exhibited a remarkable PCE of 21%. Other candidate metals that have been used to replace lead include tin, copper, and antimony (Li & Gao, 2020; Boopathi et al., 2017). Among these lead-free alternatives, tin-based perovskites are the best alternative due to their narrow bandgap, similar chemical properties to lead, and also PCE values exceeding those of other lead-free perovskites (Boopathi et al., 2017; Jiang et al., 2020; Qian et al., 2016).

Although tin-based perovskite cells have been favored, these cells still face problems such as instability (as Sn^{2+} can easily be oxidized to $Sn^{4+,}$ when exposed to air) (Zhao et al., 2017), high carrier recombination rates (due to high doped hole concentrations of the order of 1019 cm^3) (Wu et al., 2017) difficulty in controlling the morphology during processing (due to the rapid reaction between SnI_2 and ammonium salts) (Zhao et al., 2017; Wu et al., 2017; Hao et al., 2015) and poor electronic band alignment between the electron transport layer (ETL), Sn-based absorber and hole transport layer (HTL) (Zhao et al., 2017). Some successful strategies have been introduced to reduce tin oxidation. For example, tin (II) fluoride (SnF_2) was added to the perovskite material, which reduced both the instability and the doped hole density, resulting in better performance (Kumar et al., 2014; Lee et al., 2016). Despite the fact that $CH_3NH_3SnI_3$ is widely used as an absorption material due to its interesting absorption properties, it faces a particular problem of temperature instability, which is related to the organic cation $(CH_3NH_3)^+$ (Hao et al., 2014; Rono et al., 2021). It has been found that when formamidinium $(HC(NH_2)_2)^+$ is used instead of methylammonium $(CH_3NH_3)^+$, a more compact stable solid perovskite is formed (Amat et al., 2014).

By combining the results of theoretical calculations and simulations with experimental data, Qian et al (Qian et al., 2016) provided a clear overall picture for the properties of halogenated perovskites ABX_3 (A = CH_3NH_3, $CH(NH_2)_2$, Cs, Rb; B= Pb, Sn, Ge; X = I, Br, Cl, F). Referring to the PCEs of halide perovskites simulated by the Shockley-Queisser Maximum Solar Cell Efficiency (S-Q) model under AM1.5 G illumination, the results indicate that the PCEs of (ABX_3) perovskites increase from Cl to Br to I, as the band gap becomes narrower when X increases from Cl to Br to I. Since $HC(NH_2)_2SnI_3$ remains one of the most promising lead-free perovskite candidates due to its ideal bandgap and good charge transport (Qian et al., 2016), it is therefore necessary to carefully study the various parameters of the architecture of these cells to further improve their overall performance.

With this in mind, we therefore thought of studying the effect of high temperature on the PV performance of a solar cell based on the formamidinium tin iodide perovskite $HC(NH_2)_2SnI_3$ (the perovskite which is at the top of the ranking thanks to its high efficiency) using the one-dimensional numerical simulator of solar cells, SCAPS-1D (Solar Cell Capacitance Simulator) (Burgelman et al., 2021). The cell to be studied has the following general architecture: glass/FTO/WS_2/$HC(NH_2)_2SnI_3$/Cu_2O/Au; We therefore plan to analyze the effect of temperature on this structure, on the nature of the HTL layer and the effect of the modification of the contact of the back metal.

Numerical Simulation

We use SCAPS-1D to simulate the solar cells based on the formamidinium tin iodide perovskite $HC(NH_2)_2SnI_3$. This software is based on general semiconductor physics, such as the Poison equation, the drift diffusion

equation, and the continuity equation for electrons and holes. The basic equations are usually solved in 1D under a steady-state condition. We illustrate the solar cell configuration to be studied in Figure 1-a: the adopted cell is a P-I-N device structured as follows: glass/FTO/WS_2/$HC(NH_2)_2SnI_3$/Cu_2O/Au. The corresponding band alignments between the ETL layer, the perovskite and the proposed HTL layer in this primary structure are also shown in Figure 1-b.

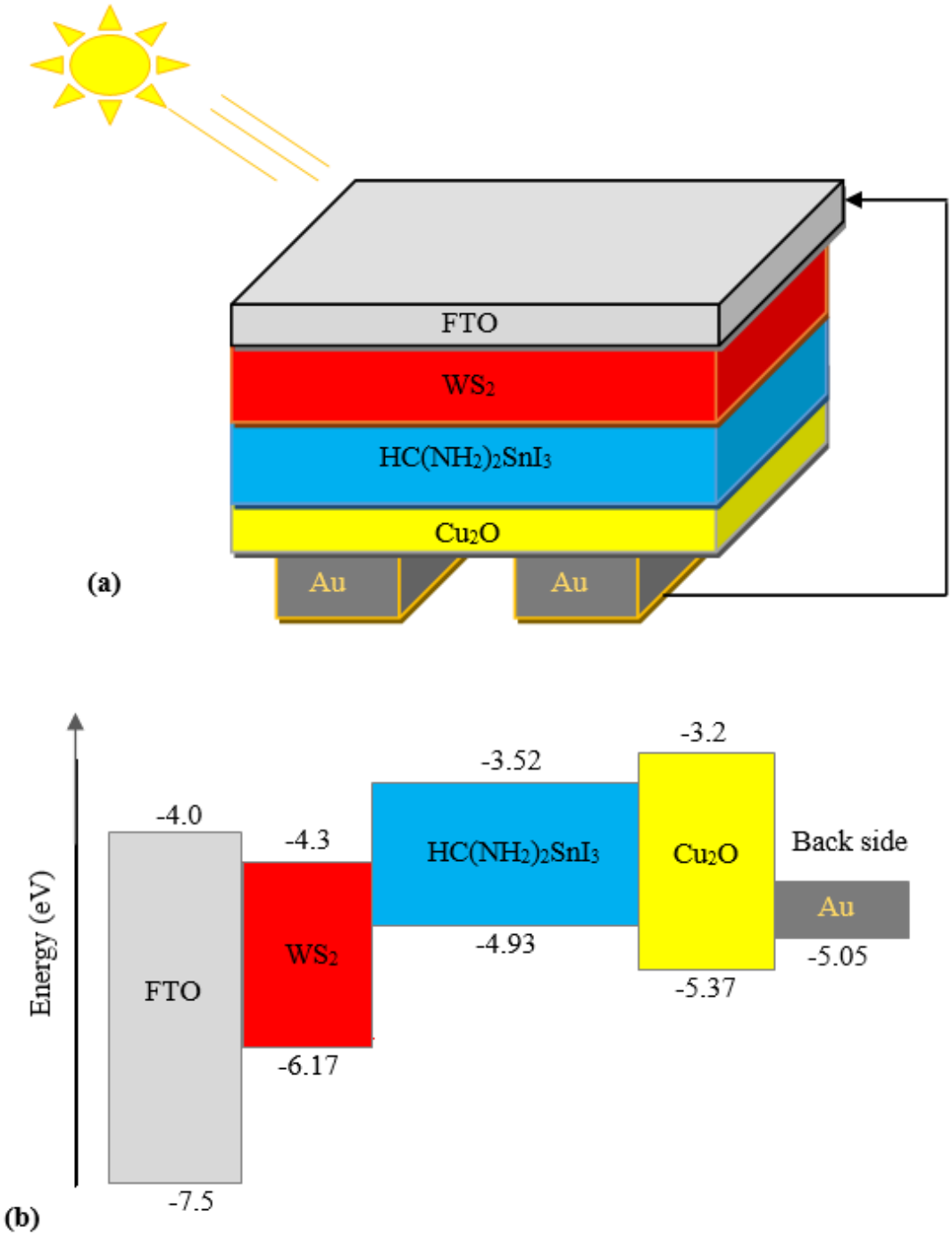

Figure 1.a) Primary device structure of the adopted PSC cell: FTO as window layer, WS_2 as ETL layer, $HC(NH_2)_2SnI_3$ perovskite as absorber, Cu_2O as HTL layer and Au as back contact. b) Corresponding energy band diagram.

The N part is the ETL layer, which in this case is tungsten disulfide WS_2, the I part is the absorber: the formamidinium tin iodide perovskite $HC(NH_2)_2SnI_3$ which can be denoted FASnI3, and the P part is the HTL layer which is copper(I) oxide Cu_2O. Tungsten disulfide was chosen as the ETL due to its inherent optoelectronic properties: band gap between 1.33 and 2.2 eV, high electron transport mobility (approximately 260 $cm^2\ V^{-1}\ s^{-1}$), and high transparency (Hankare et al., 2009). In addition, formamidinium tin iodide was also

-7.5

considered as an ideal absorber due to its good light absorption (band gap of 1.41 eV) and relatively high thermal stability (Amat et al., 2014). Copper(I) oxide was chosen as a representative of the inorganic HTL materials. This material (Cu_2O) exhibits better band alignment with perovskite, high hole mobilities (about 80 cm^2 V^{-1} s^{-1}) (Kanoun et al., 2019) and solution transformable and exhibits high optical transparency (Guo et al., 2017).

Ideally, when the device is under illumination, light is absorbed by the perovskite layer and electron-hole pairs, also called excitons, are generated. These charges move towards the electrodes by diffusion-controlled processes: at the ETL and perovskite layer boundary, electrons dissociate from holes and are transferred to the metal contact. Similarly, at the perovskite and HTL boundary, holes separate from electrons and are transferred by HTL to the back metal contact. It is important to emphasize that these processes have a significant impact on the PCE of the device (Rono et al., 2021; Yang et al., 2016).

Input Parameters of the Primary Device

The input parameters describing the adopted primary device FTO/WS_2/$HC(NH_2)_2SnI_3$/Cu_2O/Au were reported from recently published experimental and theoretical data. We give the thicknesses of each layer of the adopted configuration and these of electrical parameters in Table 1. The thermal velocities of holes and electrons were assumed constant and fixed at a value of 107 cm s^{-1}.

Table 1. Electrical parameters of the structure were adopted in Figure 1.a

Input parameter	FTO [a]	WS_2 (ETL)[b]	$HC(NH_2)_2SnI_3$ (absorbeur)[c]	Cu_2O (HTL)[a]
Thickness, $e(\mu m)$	0.04	2	0.8	0.05
Band gap, $E_g\,(eV)$	3.5	1.87	1.41	2.17
Affinity, $\chi(eV)$	4.0	4.3	3.52	3.2
Relative Dielectric permittivity, ε_r	9.0	11.9	8.2	7.11
CB effective density of states, $N_c(cm^{-3})$	2.2×10^{18}	1.0×10^{18}	1.0×10^{18}	2.02×10^{17}
VB effective density of states, $N_v(cm^{-3})$	1.8×10^{19}	2.4×10^{19}	1.0×10^{18}	1.1×10^{19}
Electron mobility, $\mu_e(cm^2V^{-1}s^{-1})$	20.0	260	22	200
hole mobility, $\mu_h(cm^2V^{-1}s^{-1})$	10.0	51	22	80
Density of n-type doping, $N_D(cm^{-3})$	1.0×10^{19}	1.1×10^{19}	0.0	0.0
Density of p-type doping, $N_A(cm^{-3})$	0.0	0.0	7.0×10^{16}	1.0×10^{18}
Density of defect, $N_t(cm^{-3})$	0.0	1.2×10^{11}	2.0×10^{15}	1.0×10^{14}

[a] (Kanoun et al., 2019)
[b] (Kumar & Singh, 2020)
[c] (Abdelaziz et al., 2020)

We note that the default solar irradiance integrated in the SCAPS-1D software is AM1.5G with an intensity of 100 mW cm^{-2} and the frequency is 106 Hz.

Basic Equations

The SCAPS-1D software (Burgelman et al. 2021**)** solves, numerically, the basic differential equations governing semiconductors in steady-state operation. It defines the physics of the modeled device, such as the recombination profile, electric field distribution, and current densities. The essential differential equations for semiconductors are Poisson's equation (1) and continuity equation for holes and electrons equation (2): (Sobayel et al., 2019).

$$\frac{d^2\psi}{dx^2} = \frac{e}{\varepsilon_0\varepsilon_r}\left[p(x) - n(x) + N_D - N_A + \rho_p - \rho_n\right] \quad (1)$$

Where ψ is electrostatic potential, n and p are electron and hole concentrations, ε_0 is vacuum and ε_r is relative permittivity, N_D and N_A are donor and acceptor doping density, ρ_n , ρ_p are electrons and holes distribution.

$$\frac{dJ_p}{dx} = \frac{dJ_n}{dx} = G - R \tag{2}$$

Where G is generation rate and R is recombination rate, J_p and J_n are holes and electron current densities. Carrier transport occurs according to the following drift and diffusion equations:

$$J_n = \mu_n n \frac{d\psi}{dx} + D_n \frac{dn}{dx} \tag{3}$$

$$J_p = \mu_p p \frac{d\psi}{dx} + D_p \frac{dp}{dx} \tag{4}$$

Results and Discussion

Effect of Temperature on Primary Structure

As a first step, we study the effect of temperature on the performance of the solar cell having the configuration: glass/FTO/WS_2/$HC(NH_2)_2SnI_3$/Cu_2O/Au, which we call the primary structure. We consider a wide temperature range from 250 to 600 K. We plot the I-V characteristic influenced by these temperatures in Figure 2.

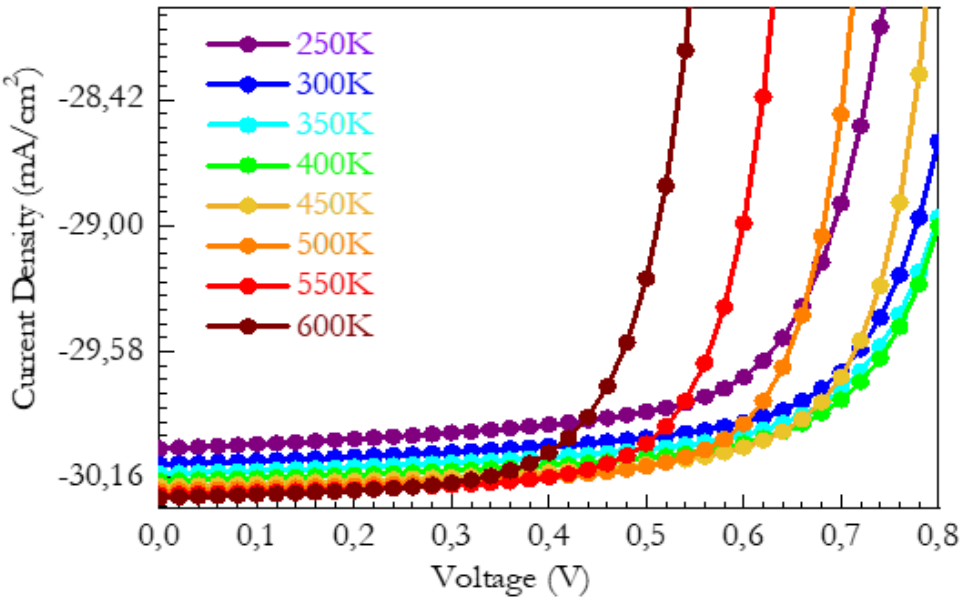

Figure 2. Variation of the current-voltage characteristic under the effect of temperature

The variations in the primary PSC performance parameters Voc, Jsc, FF, and PCE due to the temperature variation from 250 to 600 K are shown in Figure 3 (a-d) respectively. We note, through the analysis of the I-V characteristic curves obtained shown in Figure 2 and through the PV performances shown in Figure 3, that when the temperature increases from 250K to 350K, the current increases very slightly in an exponential manner and the open circuit voltage also increases. Whereas when the temperature increases from 350K to 600K, the current still increases in the same proportionality, but the open circuit voltage decreases considerably.

In terms of the grading: we can therefore say that under the effect of a temperature increase from 250K to 350K, the voltage of this primary cell gains 16.44 mV/K (or +0.53%) and it loses 9.66 mV/K (or –0.31%) beyond 350K (i.e., beyond 76.85°C). As for the current, it gains a slight intensity of approximately 6.10-4 mA/cm^2/K (or +0.002%). This can be explained by good light absorption. Unlike the behavior of the open-circuit voltage, the form factor decreases up to 350K and then increases considerably beyond this temperature value (see Figure 3-c). Regarding the PCE energy conversion efficiency of this primary cell, it increases by 0.022%/K when the temperature rises from 250K to 300K, then remains relatively constant from 300K to 389K and then decreases by 0.037%/K from 389K to 600K (see Figure 3-d). We also note that the maximum conversion efficiency of this primary cell is 23.24% at 389K.

From the results obtained, we can deduce that the solar cell based on the formamidinium tin iodide perovskite $FASnI_3$ designed as an absorber layer between the ETL layer, formed by tungsten disulfide WS_2, and the HTL layer formed by copper (I) oxide Cu_2O, represents high photovoltaic performances: High efficiency up to 389 K (115.85 °C) and the temperature increase by 1 K causes an efficiency decrease of only 0.037% (i.e. - 0.16% compared to the maximum efficiency) in the temperature range between 389 K and 600 K.

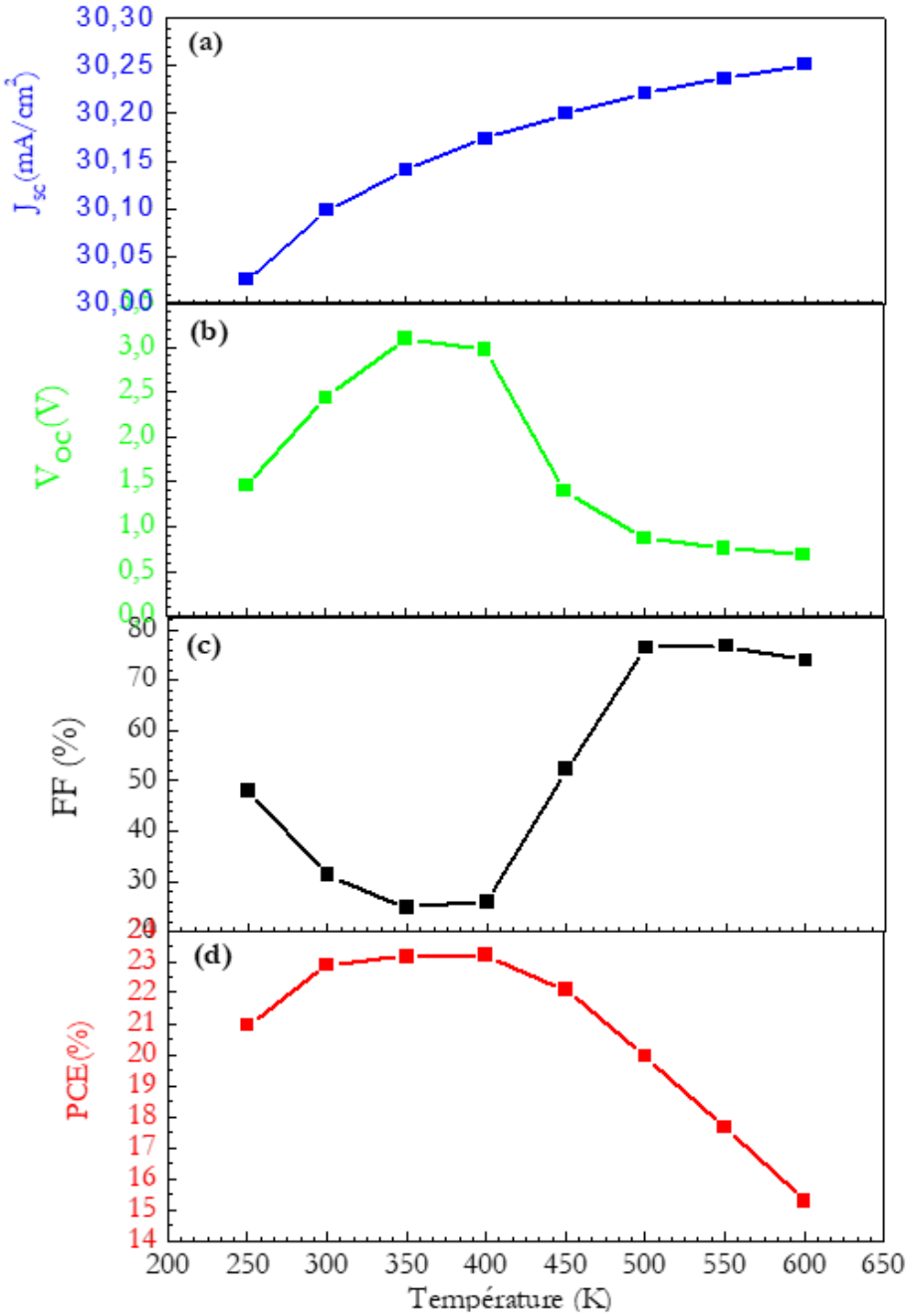

Figure 3. Variation of photovoltaic performance of the primary cell: FTO/WS_2/$HC(NH_2)_2SnI_3$/Cu_2O /Au, as a function of temperature: a) short-circuit current density, b) open-circuit voltage, c) form factor and d) efficiency.

Effect of Temperature on the Nature of the HTL Layer

In this part, we substitute the inorganic semiconductor Cu_2O of the HTL layer by 6 other materials, 3 of them are organic semiconductors: Spiro-OMeTAD, P3HT and D-PTTT-14, and 3 are inorganic semiconductors: CuSCN, MoO_3 and NiO (see Figure 4). We therefore study the effect of temperature on the 6 solar cells obtained based on these semiconductors. The input parameters describing these HTL layer materials are summarized in Table 2 (for organic and inorganic HTL layers):

Table 2. Input parameters of the different used HTL

Input parameter	Organic HTLs			Inorganic HTLs		
	Spiro-OMeTAD[a]	P3HT[d]	D-PBTTT-14[a]	CuSCN[d]	NiO[e]	MoO_3[f]
Thickness, $e(\mu m)$	1.0	0.05	0.003	0.05	0.05	0.05
Band gap, $E_g\ (eV)$	3.06	1.85	2.16	3.4	3.8	3
Affinity, $\chi(eV)$	2.05	3.1	3.2	1.9	1.46	2.5
Relative Dielectric permittivity, ε_r	3.0	3.4	10	10	10.7	12.5
CB effective density of states, $N_c(cm^{-3})$	2.8×10^{19}	1.0×10^{22}	2.8×10^{19}	1.7×10^{19}	2.8×10^{19}	2.2×10^{18}
VB effective density of states, $N_v(cm^{-3})$	1.0×10^{19}	1.0×10^{22}	1.0×10^{19}	2.5×10^{21}	10^{19}	1.8×10^{19}
Electron mobility, $\mu_e(cm^2V^{-1}s^{-1})$	1.0×10^{-4}	1.0×10^{-4}	2.83×10^{-3}	1.0×10^{-4}	12	25
hole mobility, $\mu_h(cm^2V^{-1}s^{-1})$	2.0×10^{-4}	1.0×10^{-3}	2.83×10^{-3}	1.0×10^{-1}	2.8	100
Density of n-type doping, $N_D(cm^{-3})$	0.0	0.0	0.0	0.0	0.0	0.0
Density of p-type doping, $N_A(cm^{-3})$	1.0×10^{18}	3.17×10^{13}	1.0×10^{18}	1.0×10^{18}	10^{18}	10^{18}
Density of defect, $N_t(cm^{-3})$	2.0×10^{14}	1.0×10^{14}	1.0×10^{14}	1.0×10^{14}	10^{15}	10^{15}

[a] (Kanoun et al., 2019)
[d](Azri et al., 2019)
[e] (Hossain,. et al 2015)
[f] (Li et al., 2019)

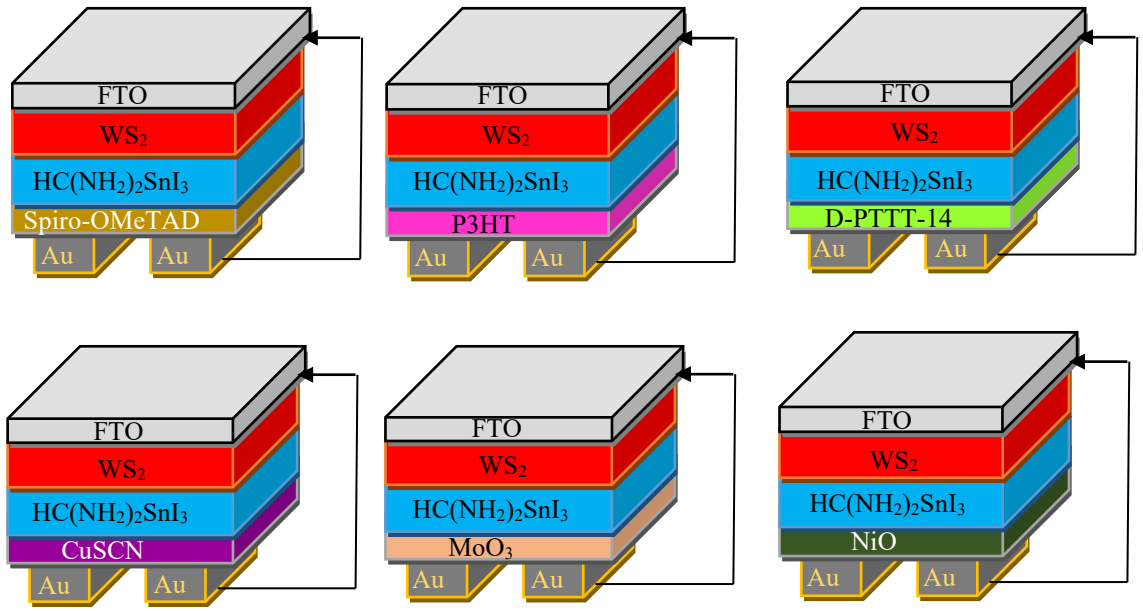

Figure 4. Structures of the (6) studied configurations in which the primary cell's HTL of Cu_2O of was replaced with Spiro-OMeTAD, P3HT, D-PTTT-14, CuSCN, MoO_3 and NiO.

We present the PV performances of the six cells studied in Figure 5 and we note the following points through the analysis of these performances:

- For the open circuit voltage, the behavior of the six (6) cells studied is similar to that of our primary solar cell based on Cu_2O, suitably to the relationship $V_{oc} = \frac{nK_B T}{q} \ln\left[\frac{I_{ph}}{I_s} + 1\right]$, but we notice that the value of this voltage is lower for the organic layers.
- The current density of the organic material D-PTTT-14 is completely different from that of other used materials.
- Unlike the behavior of the open-circuit voltage, the form factor decreases up to 350 K, increases up to 500 K, and then decreases again beyond this value, according to the relationship $FF = \frac{P_{max}}{I_{sc} \times V_{oc}}$, except for the D-PTTT-14-based HTL, which is different to the other layers.

For the performance we note that the behavior of HTL layers based on inorganic materials is identical to that of our studied cell based on Cu_2O, but this is not the case for organic HTL layers. We conclude that the three (3) cells based on inorganic materials have high performance compared to those based on organic materials. Table 3

summarizes the maximum efficiencies obtained for the seven cells studied. We also report at what temperature these efficiencies were achieved.

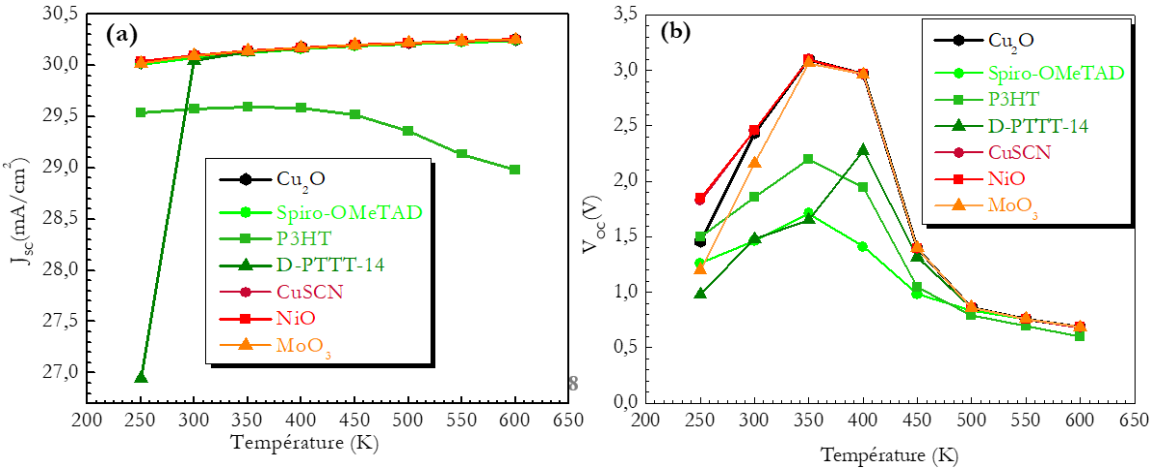

Figure 5. Effect of variation in the nature of the HTL layer as a function of temperature: a) Jsc, b) Voc, c) FF and d) PCE

Table 3. Maximum efficiency of the 7 studied cells consisting of Cu_2O, CuSCN, NiO, MoO_3, Spiro-OMeTAD, P3HT and D-PTTT-14 as HTLs and WS_2 as ETL.

Solar cells	Cu_2O	CuSCN	NiO	MoO_3	Spiro-OMeTAD	P3HT	D-PTTT-14
PCE (%)	23.24	23.24	23.24	23.23	21.75	22.05	22.85
Température (K)	389	387	388	390	373	373	405

We can conclude that these devices are resistant to high temperatures; they can therefore be used in very hot regions such as the Sahara, in hybrid photovoltaic-thermal sensors and even in space applications.

Effect of Back Contact Metal

In this section, we study, at room temperature (300K), the effect of the nature of the metal's back contact on the efficiency of our primary solar cell with the following structure: glass/FTO/WS_2/$HC(NH_2)_2SnI_3$/Cu_2O/Au. We therefore replace gold (Au) with other metals: platinum Pt, palladium Pd, nickel Ni, silver Ag, and copper Cu, and we determine the efficiency corresponding to each of these metals. To do this, we will need to introduce the work function values for these metals (see Table 4).

Table 4. Input parameter for different metals and corresponding PCE

Metal	Au	Pt	Pd	Ni	Ag	Cu
Work function (eV)	5.05	5.65	5.3	5.0	4.7	4.65
PCE (%)	22.89	22.89	22.89	22.89	19.06	17.72

Based on the results obtained (Table 4), we deduce that we can achieve the same efficiency as gold (Au) using the following metals: platinum (Pt), palladium (Pd), and nickel (Ni). To further minimize the cost of PSCs, it is therefore possible to use a contact metal that is less expensive than gold, such as platinum and nickel. If we are interested in moving towards healthy, clean energy, it is advisable to use platinum, given the toxicity of nickel.

Conclusion

In this paper, we analyzed the effect of temperature on the PV performance of a solar cell based on halogenated formamidinium tin iodide perovskite using the SCAPS-1D simulator. Six organic and inorganic semiconductor materials were inserted as a hole transport layer (HTL) in the primary cell FTO/WS_2/$HC(NH_2)_2SnI_3$/Cu_2O/Au, maintaining the primary electron transport layer (ETL). We also analyzed the effect of temperature on the six cells obtained based on these materials.

The simulation results show that the PCE energy conversion efficiencies of devices based on the inorganic materials Cu_2O, CuSCN, NiO, and MoO_3 are all similar (23.24%) and significantly higher than those based on the organic materials Spiro-OMeTAD, P3HT, and D-PTTT-14. This efficiency was achieved at 389K (115.85°C). Of course, cheaper and non-toxic metals such as Platinum can be used, in back contact, to replace gold, since they provide the same performance as the latter.

Scientific Ethics Declaration

* The authors declare that the scientific ethical and legal responsibility of this article published in EPSTEM journal belongs to the authors.

Conflict of Interest

* The authors declare that they have no conflicts of interest

Funding

* This research received no specific grant from any funding agency in the public, commercial, or not-for-profit sectors.

Acknowledgements or Notes

* This article was presented as an oral presentation at the International Conference on Technology, Engineering and Science (www.icontes.net) held in Antalya/Türkiye on November 12-15, 2025.

* The authors are thankful to Professor Marc Burgelman and his coworkers at the University of Ghent, Belgium, for providing the SCAPS-1D software used in this study.

References

Abdelaziz, S., Zekry, A., Shaker, A., & Abouelatta, M. (2020). Investigating the performance of formamidinium tin-based perovskite solar cell by SCAPS device simulation. *Optical Materials, 101*, 109738.

Amat, A., Mosconi, E., Ronca, E., Quarti, C., Umari, P., Nazeeruddin, M. K., & De Angelis, F. (2014). Cation-induced band-gap tuning in organohalide perovskites: Interplay of spin–orbit coupling and octahedra tilting. *Nano Letters, 14*(6), 3608-3616.

Ashrafi, S. S., Hossain, K., Ahmed, F., Hossain, A., & Rahman, O. (2020). Fabrication and characterization of graphene incorporated Cu based perovskite in application of perovskite solar cell under ambient condition. *Advances in Materials Physics and Chemistry, 10*(1), 1.

Azri, F., Meftah, A., Sengouga, N., & Meftah, A. (2019). Electron and hole transport layers optimization by numerical simulation of a perovskite solar cell. *Solar Energy, 181*, 372-378.

Boopathi, K. M., Karuppuswamy, P., Singh, A., Hanmandlu, C., Lin, L., Abbas, S. A., Chang, C. C., Wang, P. C., Li, G., & Chu, C. W. (2017). Solution-processable antimony-based light-absorbing materials beyond lead halide perovskites. *Journal of Materials Chemistry A, 5*, 20843-20850.

Burgelman, M., Decock, K., Niemegeers, A., Verschraegen, J., & Degrave, S. J. F. (2021). *SCAPS manual*.

Filip, M. R., Eperon, G. E., Snaith, H. J., & Giustino, F. (2014). Steric engineering of metal-halide perovskites with tunable optical band gaps. *Nature Communications, 5*(1), 19.

Guo, Y., Lei, H., Xiong, L., Li, B., Chen, Z., Wen, J., & Fang, G. (2017). Single phase, high hole mobility Cu2O films as an efficient and robust hole transporting layer for organic solar cells. *Journal of Materials Chemistry A, 5*(22), 11055-11062.

Hankare, P. P., Manikshete, A. H., Sathe, D. J., Chate, P. A., Patil, A. A., & Garadkar, K. M. (2009). WS2 thin films: Opto-electronic characterization. *Journal of Alloys and Compounds, 479*(1-2), 657-660.

Hao, F., Stoumpos, C. C., Cao, D. H., Chang, R. P., & Kanatzidis, M. G. (2014). Lead-free solid-state organic-inorganic halide perovskite solar cells. *Nature Photonics, 8*(6), 489-494.

Hao, F., Stoumpos, C. C., Guo, P., Zhou, N., Marks, T. J., Chang, R. P., & Kanatzidis, M. G. (2015). Solvent-mediated crystallization of CH3NH3SnI3 films for hetero junction depleted perovskite solar cells. *Journal of the American Chemical Society, 137*(35), 11445-11452.

Hossain, M. I., Alharbi, F. H., & Tabet, N. (2015). Copper oxide as inorganic hole transport material for lead halide perovskite based solar cells. *Solar Energy, 120*, 370-380.

Hu, W., He, X., Fang, Z., Lian, W., Shang, Y., Li, Y., & Yang, S. (2020). Bulk heterojunction gifts bismuth-based lead-free perovskite solar cells with record efficiency. *Nano Energy, 68*, 104362.

Jiang, X., Wang, F., Wei, Q., Li, H., Shang, Y., Zhou, W., & Ning, Z. (2020). Ultra-high open-circuit voltage of tin perovskite solar cells via an electron transporting layer design. *Nature Communications, 11*(1), 1-7.

Kamat, P. V., Bisquert, J., & Buriak, J. (2017). Lead-free perovskite solar cells. *ACS Energy Letters, 2*, 904-905.

Kanoun, A. A., Kanoun, M. B., Merad, A. E., & Goumri-Said, S. (2019). Toward development of high-performance perovskite solar cells based on CH3NH3GeI3 using computational approach. *Solar Energy, 182*, 237-244.

Kumar, M. H., Dharani, S., Leong, W. L., Boix, P. P., Prabhakar, R. R., Baikie, T., & Mathews, N. (2014). Lead-free halide perovskite solar cells with high photocurrents realized through vacancy modulation. *Advanced Materials, 26*(41), 7122-7127.

Kumar, S. S. (2020). Synthesis and characterization of lead free perovskite solar cells. *Materials Today: Proceedings, 26*, 2574-2579.

Kwak, J. I., Nam, S. H., Kim, L., & An, Y. J. (2020). Potential environmental risk of solar cells: Current knowledge and future challenges. *Journal of Hazardous Materials, 392*, 122297.

Lee, S. J., Shin, S. S., Kim, Y. C., Kim, D., Ahn, T. K., Noh, J. H., & Seok, S. I. (2016). Fabrication of efficient formamidinium tin iodide perovskite solar cells through SnF2–pyrazine complex. *Journal of the American Chemical Society, 138*(12), 3974-3977.

Li, G. R., & Xue, P. G. (2020). Low-cost counter-electrode materials for dye-sensitized and perovskite solar cells. *Advanced Materials, 32*(3), 1806478.

Li, W., Li, W., Feng, Y., & Yang, C. (2019). Numerical analysis of the back interface for high efficiency wide band gap chalcopyrite solar cells. *Solar Energy, 180*, 207-215.

Perl, E. E., Simon, J., Geisz, J. F., Lee, M. L., Friedman, D. J., & Steiner, M. A. (2016). Measurements and modeling of III-V solar cells at high temperatures up to 400 °C. *IEEE Journal of Photovoltaics, 6*(5), 1345-1352.

Qian, J., Xu, B., & Tian, W. (2016). A comprehensive theoretical study of halide perovskites ABX3. *Organic Electronics, 37*, 61-73.

Rono, N., Merad, A. E., Kibet, J. K., Martincigh, B. S., & Nyamori, V. O. (2021). Optimization of hole transport layer materials for a lead-free perovskite solar cell based on formamidinium tin iodide. *Energy Technology, 9*(12), 2100859.

Rono, N., Merad, A. E., Kibet, J. K., Martincigh, B. S., & Nyamori, V. O. (2021). A theoretical investigation of the effect of the hole and electron transport materials on the performance of a lead-free perovskite solar cell based on CH3NH3SnI3. *Journal of Computational Electronics, 20*(2), 993-1005.

Snaith, H. J. (2013). Perovskites: The emergence of a new era for low-cost, high-efficiency solar cells. *The Journal of Physical Chemistry Letters, 4*(21), 3623-3630.

Sobayel, K., Akhtaruzzaman, M., Rahman, K. S., Ferdaous, M. T., Al-Mutairi, Z. A., Alharbi, H. F., & Amin, N. (2019). A comprehensive defect study of tungsten disulfide (WS2) as electron transport layer in perovskite solar cells by numerical simulation. *Results in Physics, 12*, 1097-1103.

Sutton, R. J., Eperon, G. E., Miranda, L., Parrott, E. S., Kamino, B. A., Patel, J. B., & Snaith, H. J. (2016). Bandgap-tunable cesium lead halide perovskites with high thermal stability for efficient solar cells. *Advanced Energy Materials, 6*(8), 1502458.

Wang, Z., Lin, Q., Chmiel, F. P., Sakai, N., Herz, L. M., & Snaith, H. J. (2016). Efficient ambient-air-stable solar cells with 2D–3D heterostructured butylammonium-caesium-formamidinium lead halide perovskites. *Nature Energy, 2*(9), 1-10.

Wu, B., Zhou, Y., Xing, G., Xu, Q., Garces, H. F., Solanki, A., & Sum, T. C. (2017). Long minority-carrier diffusion length and low surface-recombination velocity in inorganic lead-free CsSnI3 perovskite crystal for solar cells. *Advanced Functional Materials, 27*(7), 1604818.

Yang, G., Tao, H., Qin, P., Ke, W., & Fang, G. (2016). Recent progress in electron transport layers for efficient perovskite solar cells. *Journal of Materials Chemistry A, 4*(11), 3970-3990.

Zhang, H., Lu, Y., Han, W., Zhu, J., Zhang, Y., & Huang, W. (2020). Solar energy conversion and utilization: Towards the emerging photo-electrochemical devices based on perovskite photovoltaics. *Chemical Engineering Journal, 393*, 124766.

Zhao, Z., Gu, F., Li, Y., Sun, W., Ye, S., Rao, H., & Huang, C. (2017). Mixed-organic-cation tin iodide for lead-free perovskite solar cells with an efficiency of 8.12%. *Advanced Science, 4*(11), 1700204.

Zhumekenov, A. A., Saidaminov, M. I., Haque, M. A., Alarousu, E., Sarmah, S. P., Murali, B., & Bakr, O. M. (2016). Formamidinium lead halide perovskite crystals with unprecedented long carrier dynamics and diffusion length. *ACS Energy Letters, 1*(1), 32–37.

Author(s) Information

Souheyla Mamoun
University of Abou Bekr Belkaid, Faculty of Sciences, Solid State Physics Team, Theoretical Physics Laboratory, Box 119, 13000, Tlemcen, Algeria
Contact e-mail: *souhila.mamoun@univ-tlemcen.dz*

Abdelkrim Elhasnaine Merad
University of Abou Bekr Belkaid, Faculty of Sciences, Solid State Physics Team, Theoretical Physics Laboratory, Box 119, 13000, Tlemcen, Algeria.

Feriel Saidi
University of Abou Bekr Belkaid, Faculty of Sciences, Solid State Physics Team, Theoretical Physics Laboratory, Box 119, 13000, Tlemcen, Algeria

To cite this article:

Mamoun, S., Merad, A. E., & Saidi, F. (2025). Engineering next generation hole transport layers for lead free perovskite solar cells exceeding 23% power conversion efficiency. *The Eurasia Proceedings of Science, Technology, Engineering and Mathematics (EPSTEM), 38,* 630-640.